Geophysical Journal International

Geophys. J. Int. (2013) **195,** 159–175
Advance Access publication 2013 July 18

doi: 10.1093/gji/ggt253

Distribution of magnetic particulates in a roadside snowpack based on magnetic, microstructural and mineralogical analyses

Michał S. Bućko,[1,2] Olli-Pekka Mattila,[1,3] Artur Chrobak,[4] Grzegorz Ziółkowski,[4] Bo Johanson,[5] Jan Čuda,[6] Jan Filip,[6] Radek Zbořil,[6] Lauri J. Pesonen[1] and Matti Leppäranta[1]

[1] *Department of Physics, University of Helsinki, P.O. Box* 64, *Gustaf Hällströmin katu* 2, 00014 *Helsinki, Finland. E-mail: michal.bucko@helsinki.fi*
[2] *Institute of Environmental Engineering, Polish Academy of Sciences, ul. Sklodowskiej-Curie* 34, 41–819 *Zabrze, Poland*
[3] *Finnish Environment Institute (SYKE), P.O. Box* 140, *Mechelininkatu* 34a, 00251 *Helsinki, Finland*
[4] *Institute of Physics, University of Silesia, ul. Uniwersytecka* 4, 40–007 *Katowice, Poland*
[5] *Electron Optical Laboratories (EPMA, SEM-EDS), Geological Survey of Finland, P.O. Box* 96, 02151 *Espoo, Finland*
[6] *Regional Centre of Advanced Technologies and Materials, Faculty of Science, Palacky University Olomouc,* 17. *listopadu* 12, 77146 *Olomouc, Czech Republic*

Accepted 2013 June 24. Received 2013 June 24; in original form 2012 July 15

SUMMARY

Vehicle traffic is at present one of the major sources of environmental pollution in urban areas. Magnetic parameters are successfully applied in environmental studies to obtain detailed information about concentrations and quality of iron-bearing minerals. A general aim of this research was to investigate the magnetic, microstructural and mineralogical properties of dust extracted from the roadside snowpack accumulated on the side of an urban highway, northern Helsinki. Vertical snow profiles were taken at different distances (5, 10 and 15 m) from the road edge, during winter season 2010–2011. The temporal distribution of mass magnetic susceptibility (χ) of the road dust shows that the concentration of magnetic particles increases in the snowpack during winter. Roadside snowpack preserves a large fraction of the magnetic particulate until the late stages of melting and this could be considered as one of the main factors responsible for the resuspension phenomenon observed in Nordic countries. The vertical distribution of χ and SIRM (saturation isothermal remanent magnetization)/χ ratio may indicate the migration of magnetic particles down in the snowpack during melting conditions. Ultrafine to coarse-grained (superparamagnetic to multidomain) magnetite was identified as the primary magnetic mineral in all the studied road dust samples. The examined road dust contains significant amount of dia/paramagnetic minerals (e.g. quartz, albite, biotite) and the content of magnetite is relatively low (below 1 weight percent, wt%). The roadside snowpack is enriched in anthropogenic particles such as angular and spherical iron-oxides, tungsten-rich particles and sodium chloride. This study demonstrates the suitability of snow as an efficient collecting medium of magnetic particulates generated by anthropogenic activities.

Key words: Environmental magnetism; Magnetic mineralogy and petrology; Rock and mineral magnetism.

1 INTRODUCTION

Roadside snowpack is exposed to pollutant loading generated by traffic and winter road maintenance (e.g. application of de-icing agents, traction sanding). This results in the accumulation of various contaminants including polyaromatic hydrocarbons (PAH) (Hautala *et al.* 1995), sulphur and nitrogen oxides (Viskari *et al.* 1997), heavy metals (Viklander 1998, 1999), de-icing salts (Sansalone & Glenn 2002) and magnetic particles (Bućko *et al.* 2011). Road traffic causes accretion of dissolved, colloidal and suspended solids in a complex heterogeneous snow matrix (Sansalone & Glenn 2002). Since snowpack acts as a seasonal storage of contaminants it can release significant quantities of pollutants into the environment during the melting period. Although snow is widely used in anthropogenic pollution studies, little is known about the distribution, migration and release of specific pollutants from urban snowpack. Snowpack seems to be a proper matrix to analyse the deposition patterns of airborne pollutants with specific events easily sampled in well-defined intervals on the basis of meteorological data.

Magnetic parameters obtained from non-destructive, fast and low-cost measurements provide information about the sources,

localization and distribution of anthropogenic magnetic particles in the environment. Numerous studies have reported the distribution of magnetic particulates in soil exposed to road traffic (e.g. Chaparro *et al.* 2010), tree leaves (e.g. Sagnotti *et al.* 2009), snow (e.g. Bućko *et al.* 2011), terrestrial moss (Fabian *et al.* 2011), moss bags and lichens (e.g. Salo *et al.* 2012).

The main objective of this work is to monitor the temporal and spatial distribution of the magnetic particulates in a roadside snowpack situated near a highway (northern Helsinki, Finland) during winter using magnetic, microstructural and mineralogical analyses, as well as physical measurements of the snowpack.

2 METHODOLOGY

2.1 Study area and sampling

Vertical snow profiles (Fig. 1B) were excavated at an open field adjacent to the eastern edge of the highway no. 45, northern Helsinki, during winter (Fig. 1A). As described by Bućko *et al.* (2010) the speed limit on this highway is 100 km hr^{-1}, and the average traffic volume exceeds 60 000 cars per day. The snow profiles were excavated during four sampling campaigns: 2010 December 7, profiles IA–C; 2011 January 20, profiles IIA–C; 2011 March 2, profiles IIIA–C; 2011 April 6, profiles IVA and IVC. During each sampling campaign the profiles were made at the following distances from the road edge: 5 m, profiles I–IVA; 10 m, I–IIIB; 15 m, profiles I–IVC. Bulk snow samples (whole snow column down to the soil surface) with a volume of 1500 cm^3 were collected from each profile and stored in plastic bags (3 × 500 cm^3). Furthermore, individual snow layers were distinguished and similarly sampled in each snow profile on the basis of the physical properties of snow, such as density, grain size, temperature and stratification, and dark layers which suggested particular accumulation periods of road dust (Fig. 1B). A total of 140 snow samples were collected during the whole winter season. All samples were transported from the field to the laboratory in portable cool boxes at a temperature below 0 °C. Each snow sample was melted at room temperature and after the complete evaporation of water the remaining material was used for the analyses. The complete evaporation of water in each sample (500 cm^3) occurred after approximately 1 month.

2.2 Meteorological data

The Finnish Meteorological Institute (FMI) provided weather data from the weather station at Helsinki-Vantaa airport (Fig. 1), located at about 8 km north from the study site. Weather data have been taken from 2010 December 1 to 2011 May 15. The records for temperature and precipitation are shown in Fig. 2. Compared to the mean conditions, the winter of 2010–2011 was slightly colder in the Helsinki area and precipitation in December 2010–January 2011 was well above average. The winter displayed four major phases during the observation period. (1) From 2010 December 7 to around 2011 January 5. This was cold early winter, with temperature generally between −15 and −5 °C and a couple of days down to below −20°C. Precipitation was heavy, with several days more than 2.5 mm d^{-1}, and three major snowfall events occurred with more than 5.0 mm d^{-1} and with a maximum of ∼15 mm in 2 days (December 5 to 6). (2) From January 6 to around February 9 was a warm period, temperature on average above −5 °C and several days above 0 °C, but also there were two short cold spells. This period also displayed strong precipitation during the first half, with more than 4.0 mm d^{-1} for several days. (3) From mid-February to the beginning of March was a period of cold and dry weather; temperature was on average between −20 °C and −15 °C and

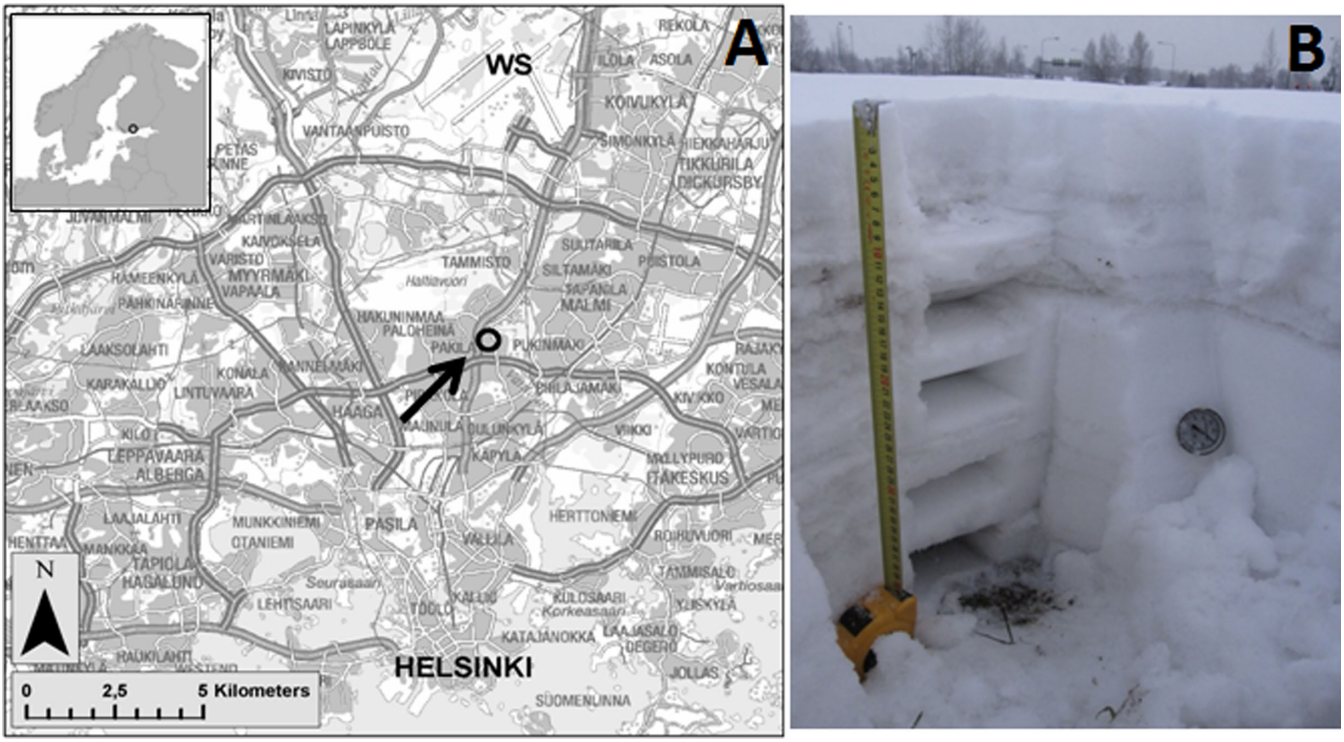

Figure 1. Map of the study area showing the roadside sampling site and the reference meteorological station (empty circle, sampling site; WS, weather station of Helsinki-Vantaa airport) (A). An example of a vertical snow profile examined at the sampling site. The picture shows the characteristic 'dark' layers suggesting a period of intense accumulation of road dust (B).

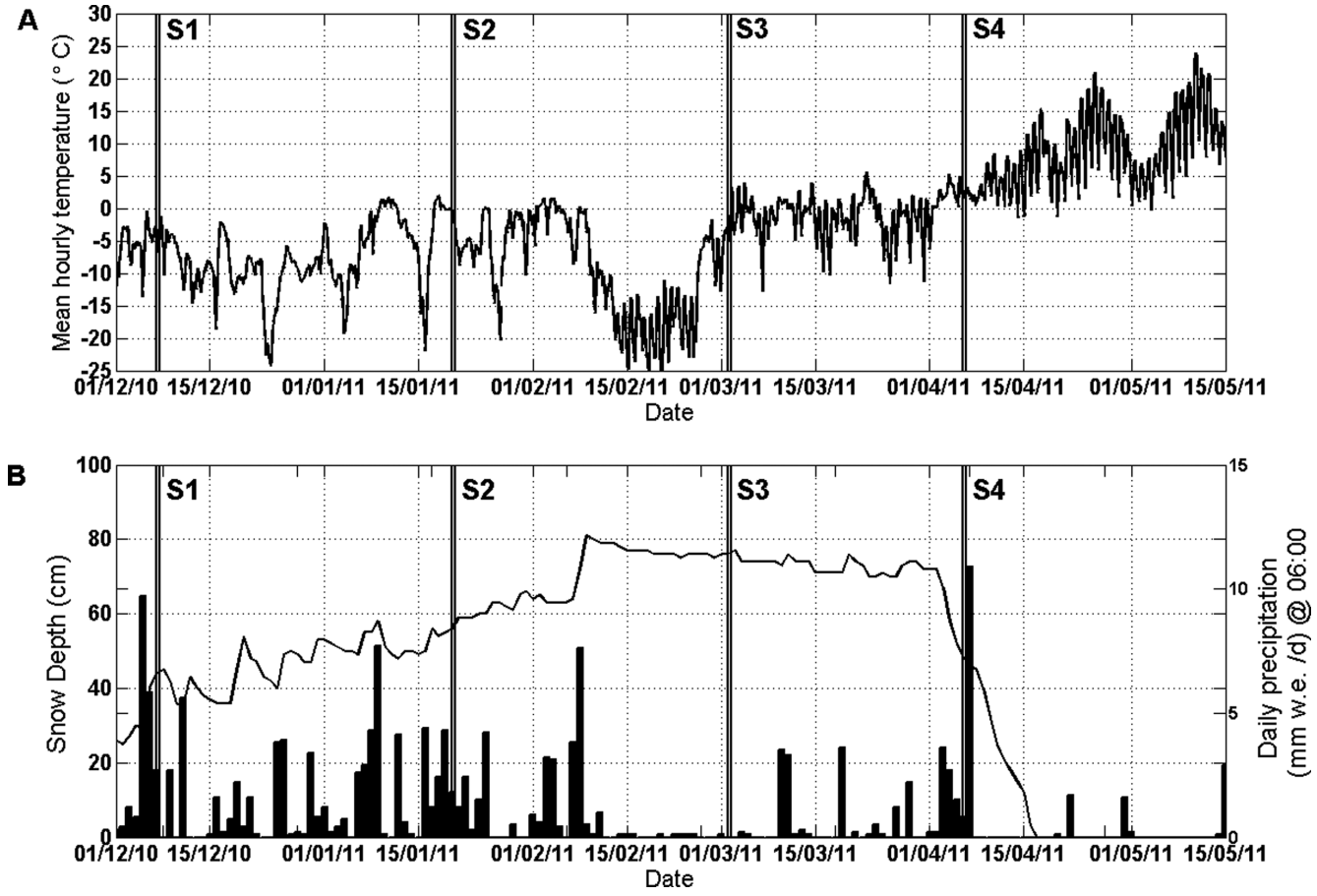

Figure 2. Weather data from meteorological station of Helsinki-Vantaa airport (provided by FMI): the four sampling campaigns are marked by letter S. Mean hourly temperature (A), Snow depth (solid line) and daily precipitation (bars) measured at 06:00 am (B).

there were no notable precipitation events. (4) The period from 2011 March 2 to the end of the experiment, showed temperature fluctuating near 0 °C. Precipitation on March 10 and 11 brought around 3.5 mm d^{-1} rain, and there was an equally strong snowfall event on March 19 and again rain on April 3 and 4, before the fourth sampling campaign.

2.3 Experimental methods

Low-field volume magnetic susceptibility (κ) of the extracted road dust was measured with a SM-100 (ZH instruments, Brno, Czech Republic, operating at 506 Hz frequency and 80 Am^{-1} field intensity) and the corresponding mass-specific susceptibility (χ) was calculated (in SI units 10^{-8} m^3 kg^{-1}) according to $\chi = \kappa/\rho$, where ρ is the bulk density, equal to sample mass divided for its volume.

The temperature dependence of κ was monitored with an Agico KLY-3S Kappabridge (Brno, Czech Republic, operating at 875 Hz frequency and 300 Am^{-1} rms field intensity) while warming samples from −195 °C (liquid nitrogen temperature) to room temperature.

Low-temperature magnetic measurements of representative samples were performed with a Superconducting Quantum Interference Device (SQUID) magnetometer (XL-7, Quantum Design, San Diego, CA, USA) in the temperature range of 2–300 K. High-temperature magnetic measurements (300–1100 K) were carried out by means of a Faraday-type magnetic balance.

Isothermal remanent magnetization (IRM) acquisition curves and hysteresis parameters such as coercivity (H_c), saturation magnetization (M_s) and saturation remanent magnetization (M_{rs}), which is equal to SIRM (saturation IRM), were measured with a Princeton Measurements Co. Vibrating Sample Magnetometer (VSM) Model 3900 (Westerville, OH, USA), with a maximum applied field of 1 T. Remanence coercivity (H_{cr}) was determined from dc demagnetization of the saturation remanence.

Selected road dust samples were investigated using a scanning electron microscope (SEM), model JEOL JSM5900 LV equipped with an energy dispersive X-ray spectrometer (EDS) with INCA Feature phase detection and classification software at the Geological Survey of Finland. The INCA Feature software performs automatic scans over the sample area and detects the grains using the backscattered electron image (recording size, shape and grey level) and subsequently analyses and classifies the phases by EDS.

Mössbauer effect measurements at 14 K and room temperature in zero magnetic field were performed on selected dust samples using Mössbauer spectrometer (Janis Research Company, Inc., Wilmington, MA, USA) with a ^{57}Co(Rh) source of γ-rays and the values of derived hyperfine Mössbauer parameters are referred to the metallic iron (α-Fe) at room temperature. Zero-field Mössbauer spectra were fitted by means of the Lorentzian line shapes using the least-square method featured in the MossWinn computer program.

The X-ray powder diffraction (XRD) pattern was recorded with a X'Pert PRO MPD (PANalytical, Almelo, The Netherlands) diffractometer (CoK_α radiation) in the Bragg–Brentano geometry,

equipped with an X′Celerator detector and programmable divergence and diffracted beam antiscatter slits. Samples were placed on a zero-background Si slides and scanned in a continuous mode (resolution of 0.017° 2 Theta). Identification of crystalline phases was done using the software High Score Plus (PANalytical) in conjunction with the PDF-4+ database.

Total contents of major and trace elements in one representative road dust sample were determined by wavelength dispersive X-ray fluorescence spectrometry (WD-XRF) using the S4 Pioneer (Bruker AXS, Karlsruhe, Germany) spectrometer. Standardless, as well as pre-calibrated GeoQuant package (Bruker AXS), based on international rock standards and internal standards were used on pressed pellet supported by H_3BO_3. Loss on ignition (LOI) was determined conventionally using laboratory balance and muffle furnace (1050 °C for 30 min).

Selected snow profiles were examined for grain size and type, layer hardness and density. The snow pits were excavated on the sampling sites situated 5 m and 10 m from the road edge. The granulometry and type of the snow were determined with a magnifying glass against a millimeter grid and classified according to Fierz *et al.* (2009). Layer hardness was determined with subjective method according to Fierz *et al.* (2009) and density measured with a container of known volume and a hand held spring scale.

3 RESULTS

3.1 Distribution of the magnetic particulate in a roadside snowpack based on magnetic (χ, SIRM/χ) and meteorological data

3.1.1 Bulk snow samples—horizontal scale

The temporal and spatial distribution of the magnetic susceptibility (χ) of the road dust accumulated in the roadside snowpack is presented in Fig. 3. The magnetic susceptibility of the powders from the bulk samples increases gradually with time, reaching the highest

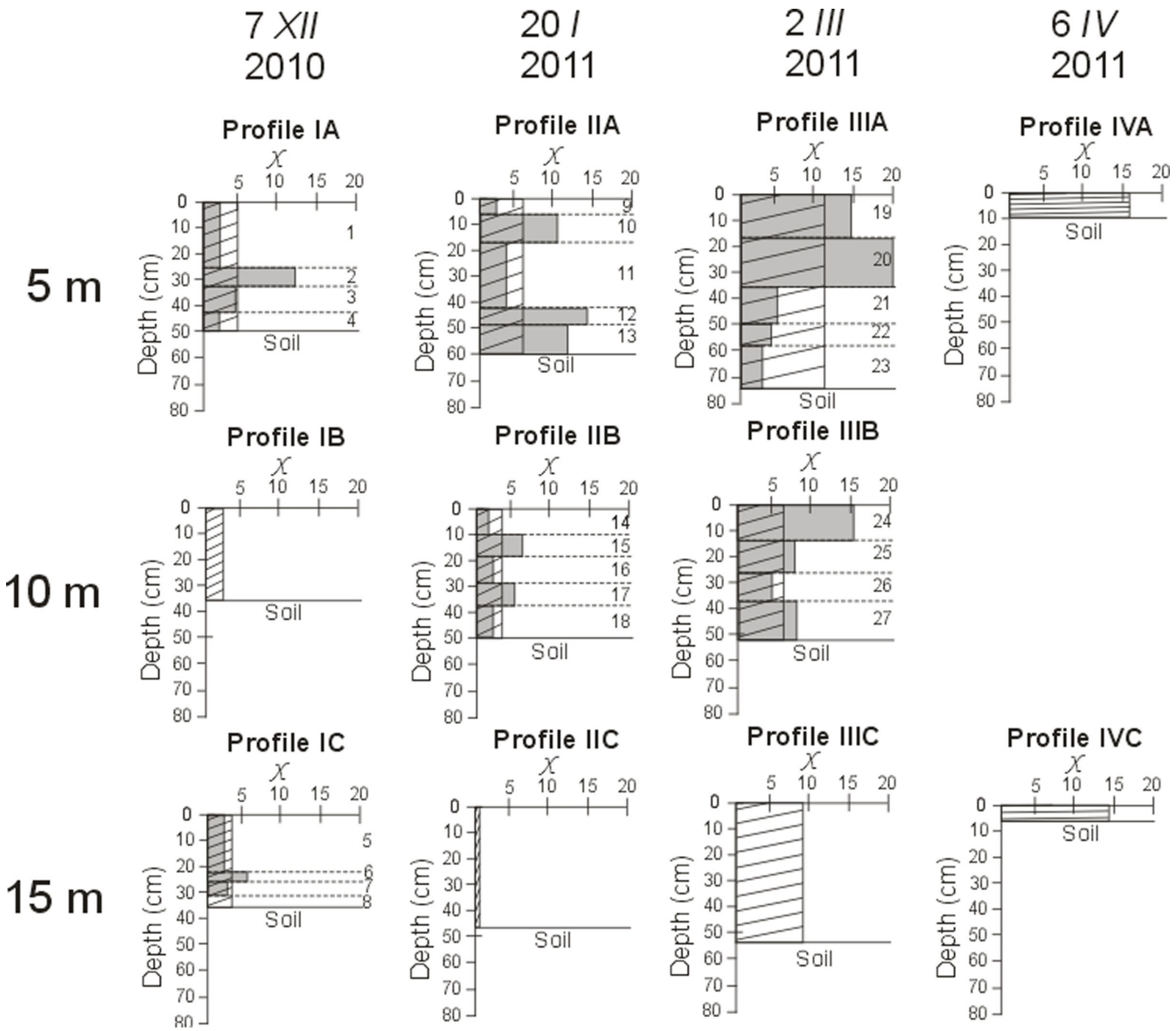

Figure 3. Mass magnetic susceptibility (χ, expressed in 10^{-8} m^3 kg^{-1}) of the road dust obtained from the bulk samples of each snow profile (transparent/lined bars) and snow layers (gray bars and Arabic numerals) collected during four sampling campaigns.

values in the samples collected during last sampling campaign—profile IVA (16.3×10^{-8} m^3 kg^{-1}) and profile IVC (14.8×10^{-8} m^3 kg^{-1}). The highest values of χ have been measured from the profiles situated at the closest distance from the road edge (profiles I–IVA). Furthermore, magnetic susceptibility decreases at 10 m distance (profiles I–IIIB) and slightly increases at 15 m from the road edge, excluding profile IIC. The ratio SIRM/χ exhibits a different horizontal distribution with respect to χ (Fig. 4). The highest values were from the powders of the profiles at 15 m from the road (profiles I–IIIC), while the lowest in profiles located at closest distance to the road (5 m, profiles I–IIIA).

The gradual increase of the snowpack thickness with time was also observed in the investigated profiles, excluding the last sampling campaign (profiles IVA and IVC were performed during late stages of melting period). The thickest snowpack was measured in profile IIIA (74 cm), and thinnest in profile IB (36 cm; Figs 3 and 4). Profiles located 5 m from the road edge are characterized by higher thickness of the snowpack than the profiles situated 10 m and 15 m from the road, possibly due to proximity of the road and microtopography.

3.1.2 Snow layers—vertical scale

The snow-fall event in early December (Fig. 2) is reflected in the distribution of magnetic susceptibility (Fig. 3). The top 25 cm of relatively fresh snow (layer 1 and 5) had not accumulated large quantities of magnetic particles, while the layers below (2 and 6), formed before the precipitation, show a higher concentration of magnetic particles, as indicated by higher values of χ. The road dust from profiles IA and IC shows a similar distribution of magnetic susceptibility, however the dust from snow layers in profile IA exhibits higher values of χ than for the profile IC. The increased values of SIRM/χ for deeper layers (Fig. 4, layers 3, 4 and 6, 7 in profiles IA and IC, respectively) may reflect higher contribution of

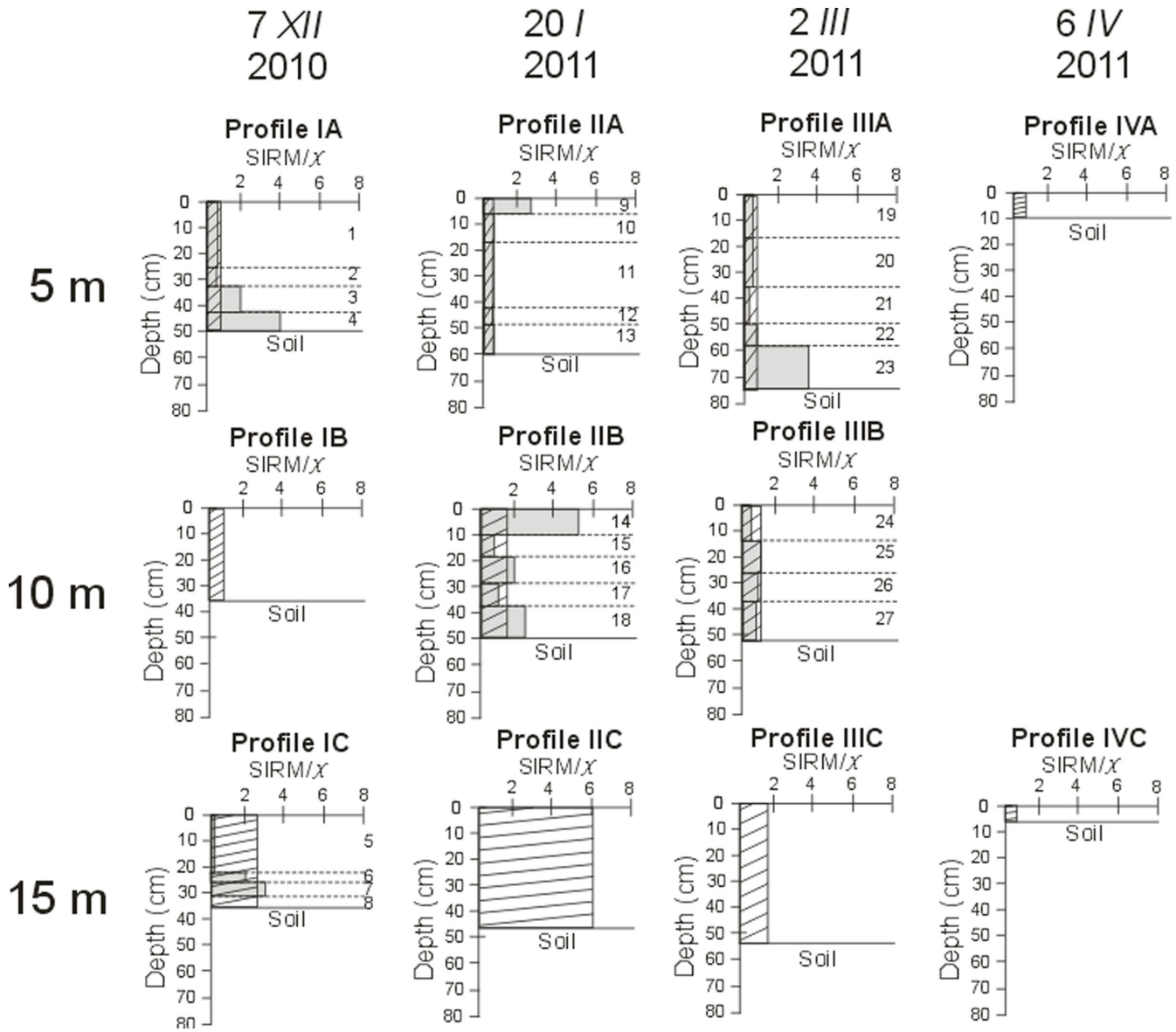

Figure 4. Ratio SIRM/χ (expressed in 10^5 Am^{-1}) of the road dust obtained from the bulk samples of each snow profile (transparent/lined bars) and snow layers (grey bars and Arabic numerals) collected during four sampling campaigns.

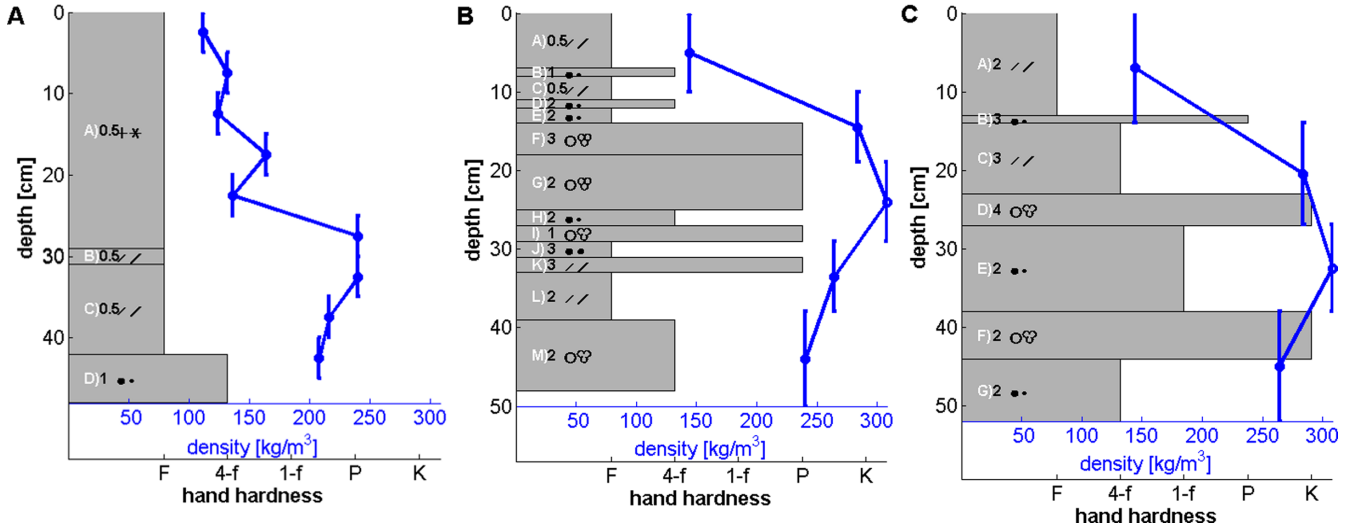

Figure 5. Profiles of grain size and type, layer hardness (according to Fierz *et al.* 2009) and density from the three observed profiles: profile IA, 7.12.2010 (A), IIB, 20.1.2011 (B) and IIIB, 2.3.2011 (C). The grain types are marked as follows: ∗ precipitation particles, / fragments of precipitation particles (of different sizes), ● rounded grains (of different sizes), ○ wet rounded grains (of different sizes), ∞ bonded ice crystals of different degree (the more connected the more bonded crystals). Hardness of deposited snow: F, very soft; 4-f, soft; 1-f, medium; P, hard; K, very hard.

finer magnetic particles than in the case of the snow layers above, suggesting migration of the finer particles down in the snowpack during melting conditions. However, the snow in layers 1 and 5 is relatively small grained and dry and has not melted after deposition (Fig. 5A). In this case, the higher values of the SIRM/χ ratio may indicate the compositional differences between dust samples obtained from top (layers 1 and 5) and bottom (layers 3, 4, 6 and 7) snow layers.

The magnetic susceptibility of road dust extracted from the top two snow layers observed during the second sampling campaign (9, 10—profile IIA and 14, 15—profile IIB), sampled in the middle of the warm period (Fig. 2), displays a similar distribution as in the top two layers of profiles performed during first sampling campaign (1, 2—profile IA and 5, 6—profile IC). The magnetic susceptibility of the powders obtained from fresh new snow (layers 9 and 14) is lower with respect to those from snow layers below (10 and 15). However, the SIRM/χ ratio is higher in the dust samples from snow layers 9 and 14 (Fig. 4). This might indicate that the fine magnetic particles in layers 9 and 14, which accumulated during the cold period between the first and second sampling campaign, had not yet migrated down in the snowpack. The low values of χ of the powders from layers 11 and 16 indicate that these are possibly the remnants of the top layer (1 and 5) observed in the previous sampling campaign. The road dust extracted from layer 11 exhibits slightly higher χ than the dust from layer 1. These differences may be associated to migration of magnetic particles with specific grain size. Conway *et al.* (1996) showed by an experiment with ash particles, that particles with diameter over 5 μm would remain immobile during melting events, whereas smaller particles migrate downwards with partially saturated water flows inside the snowpack, given moderate melt rates would apply (20–500 mm d^{-1}). This is supported by the re-frozen layers found in between 15 and 30 cm in snow profile IIB (Fig. 5B), as well as the wet snow layer at the bottom, suggesting first uniform and then preferential flow (Katsushima *et al.* 2009) and accumulation of moisture on top of frozen ground after surface melting during the week before the second sampling campaign. The distribution of χ in the two bottom layers of profile IIA (12 and 13) and IIB (17 and 18) suggests that these are the remnants of layers 2, 3 and 6, 7 observed in profiles IA and IC, respectively. However, the value of χ of the bottom layer (13) from profile IIA is significantly higher than in profile IA (3). It is possible that the bottom layer has been contaminated by the dust particles from the surface of the underlying soil.

The weather before the third sampling campaign was bi-modal with the warm period, with temperatures reaching over 0 °C from February 1 to 9, following with two weeks of very cold temperatures just before the collection of samples (Fig. 2). This period also coincides with quickly increasing solar radiation. The increasing solar radiation enhances the surface melting and favours melting in the snowpack, therefore increasing the migration and re-distribution of magnetic particles. With only a single dominating precipitation event on February 8 the snowpack does not show much increase in total depth (profiles IIIB and IIIC, Fig. 3). The top snow layers of profiles IIIA (19) and IIIB (24) show significant increase in magnetic susceptibility. The period of 2 weeks of cold temperatures and not significant precipitation triggered strong accumulation of magnetic particles in the top layer formed on February 8. The layer 20 is the remnant of layer 10 (second sampling campaign) and the road dust obtained from this layer exhibits significantly higher χ. The SIRM/χ ratio (Fig. 4) of the dust from the bottom layer of profile IIIA (23) indicates higher contribution of finer magnetic material than in the dust from the upper snow layers and this may also suggest the migration of magnetic particles with specific grain size. According to magnetic data (Fig. 3) in the profile IIIB there are clear traces (layers 25 and 27) of layers 15 and 17 (profile IIB). However this trend is not observed in the profiles situated closest to the road edge (profiles IIA and IIIA). There is no trace of layer 12 in the case of profile IIIA. This is possibly due to spatial variation between the sampling locations and/or melting which reached the bottom layers and washing out of the particles into the soil. Since the albedo of the snowpack located close to the road was lower than from farther distances, due to stronger accumulation of dust, this was likely to favour further melting. This is expressed by the growth of the snow grains, as well as higher thickness of icy layers and increased density in the snow profile IIIB (Fig. 5C).

By the fourth sampling, most of the snow had already melted and the samples were collected from patches of snow with similar distances to the road as in the earlier profiles (profile IVA and IVC). Nevertheless, the magnetic susceptibility of the road dust had still remained at a similar level as in the top layer of the profiles collected during the previous campaign. This means that some of the particles remain in the snow even after strong melting. However, low values of SIRM/χ suggest that the finer magnetic particles were washed out into the soil and the high values of χ could be related to magnetic material of coarser grain size.

3.2 Magnetic mineralogy

Low- and high-temperature magnetic measurements (Figs 6, 7 and 8C) and acquisition of IRM up to 1 T (Figs 8A and B) were used to identify the main magnetic phases in the studied road dust samples. Fig. 6 shows the magnetization dependence with temperature $M(T)$ (measurements carried out upon cooling) measured under the application of a 0.1 T magnetic field for the four representative road dust samples obtained from bulk snow samples and top snow layers of profiles IIIA and IIIB. The observed thermomagnetic curves are typically paramagnetic with a low ferromagnetic component attributed to non-zero values of the magnetization as the temperature increases. After the subtraction of the ferromagnetic contribution, the supposed paramagnetic curve fulfils the Curie law [$1/M(T)$ curves in Fig. 6] well. The high-temperature magnetic measurements allow the discrimination of the magnetic minerals according to their Curie temperatures (T_C). The $M(T)$ curves, measured up to 1100 K in a 0.1 T magnetic field indicate that magnetite is the main magnetic mineral ($T_C = 875$ K) in the road dust samples obtained both from bulk snow samples (Fig. 7A) and selected snow layers (Figs 7B and C). The enhanced magnetization at about 700 K can be attributed to some high coercive (or high anisotropy) phase in such a way that higher thermal energy causes that the corresponding magnetic moments are unblocked and follow the external magnetic field. The other possibility is a partial phase transition like crystallization or separation of magnetite that occurs during heating. Nevertheless, the ferro-para magnetic transition characteristic for magnetite is the main effect observed in the $M(T)$ curves. Magnetite is the main magnetic mineral also according to the low-temperature behaviour of the magnetic susceptibility (Fig. 8C) with an evident wide Verwey transition (from -150 °C, 123 K) characteristic for stoichiometric magnetite. The IRM curves for the bulk snow samples (Fig. 8A) as well as road dust obtained from each snow layer (Fig. 8B) saturate at about 0.2 T. This pattern indicates predominance of low-coercivity Fe-oxides (e.g. magnetite) in the roadside snowpack.

3.3 Magnetic grain size

Ratios of M_{rs}/M_s (saturation remanence/saturation magnetization) and H_{cr}/H_c (remanence coercivity/coercivity) were plotted on a Day diagram (Fig. 9) according to Day *et al.* (1977) to study the magnetic grain size dependence in road dust of all bulk samples and snow layers. The M_{rs}, M_s, H_c and H_{cr} were obtained from measurements of hysteresis loops and dc demagnetization of SIRM. Data points for all bulk samples and most of the snow layers are distributed in the pseudo-single-domain (PSD) region, close to the mixing

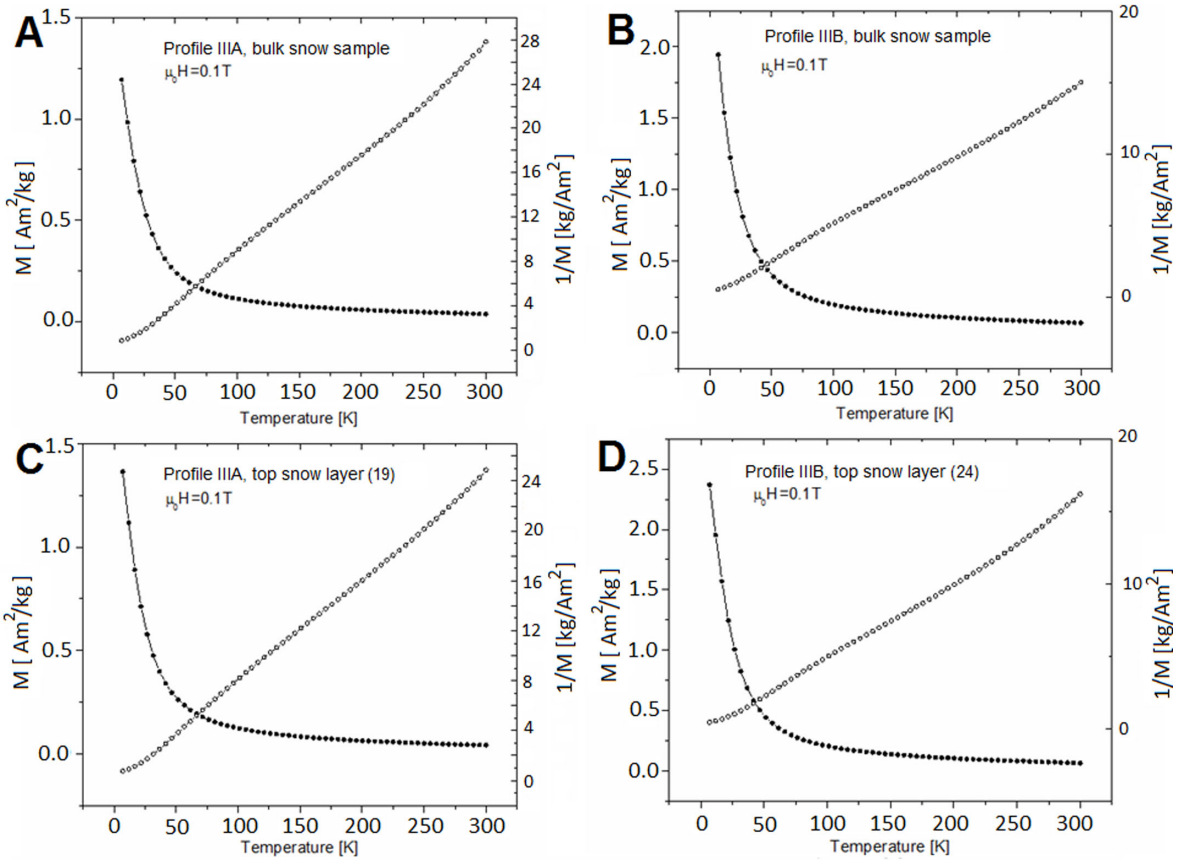

Figure 6. Magnetization M (closed circles) and inverse of the magnetization $1/M$ (open circles) versus temperature for representative road dust samples.

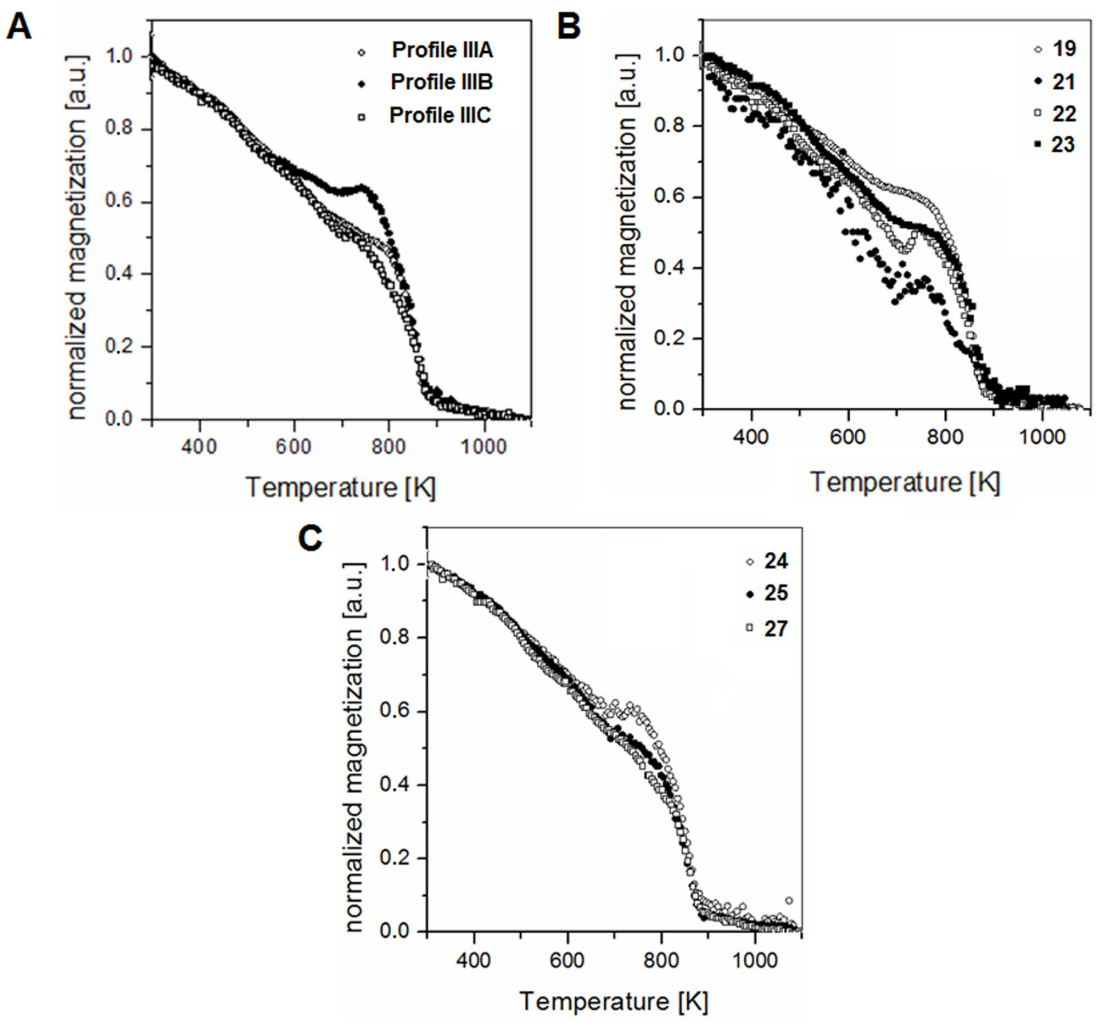

Figure 7. High temperature dependence of magnetization for the road dust obtained from selected bulk snow samples (A) and snow layers of profiles IIIA (B) and IIIB (C).

line for single-domain (SD)/multidomain (MD) and far from the SD/superparamagnetic (SP) grains.

The low-temperature magnetization measurements clearly indicate a predominant contribution of paramagnets with traces of ferromagnetic behaviour (e.g. see Fig. 11D in the next section). As it was shown (high-temperature magnetization) the ferromagnetic response is attributed to relatively low amount of magnetite grains. In this case an analysis of magnetic moments distributions was carried out making use of the Langevin granulometry methods (Kakay *et al.* 2004). The used algorithm is based on the assumption that the total magnetization is a superposition of simple Langevin functions with magnetic moments characteristic for the composing minerals (for details see Chrobak *et al.* 2011). Taking into account that the ferromagnetic signal is low, the distributions are calculated separately at $T = 2$ K and $T = 300$ K. In the first case the results are a picture of the dominating paramagnetic component. In the second case the determined distribution is attributed to magnetite grains. The calculation algorithm requires only saturated isotherms, thus in both cases unsaturated components were subtracted. The fitting error does not exceed 0.1 per cent per point for all the performed analyses. Fig. 10(A) shows a result of the Langevin granulometry analysis for the road dust sample obtained from bulk snow sample of profile IIIA (at $T = 2$ K). The distribution has a Gaussian-like shape with the maximum at about 5.5 μ_B (Bohr magneton). This value can be attributed to the iron ions in paramagnetic minerals (Parks & Akhtar 1968). Fig. 10(B) depicts a distribution of the same sample but calculated from magnetic isotherms at $T = 300$ K where the shape of distribution is rather log-normal with the maximum placed at $11 \cdot 10^3$ μ_B. This is the value of the average magnetic moment for these magnetite grains. Assuming that the molecular magnetic moment of magnetite is 3.7 μ_B and its unit cell is 0.84 nm, with eight magnetite molecules in a unit cell, the average grain size is estimated to be less than 10 nm. These kinds of nanometric magnetite grains are SP at room temperature. In conclusion, the analysed powders contain iron in the paramagnetic minerals as well as SP magnetite particles with a mean diameter of about 10 of nanometers. Figs 10(C) and (D) show the distributions of magnetic moments for road dust of bulk snow samples obtained from profile IIIB and IIIC, respectively. In a comparison with the distribution presented in Fig. 10(B), a decrease of the maximum to 10^4 μB was observed, as well as slightly broadening of their shapes.

3.4 Mass-magnetic susceptibility and magnetite content

The magnetite content was estimated from the ferromagnetic components of magnetic isotherms $M(H)$ (measured at $T = 300$ K) with

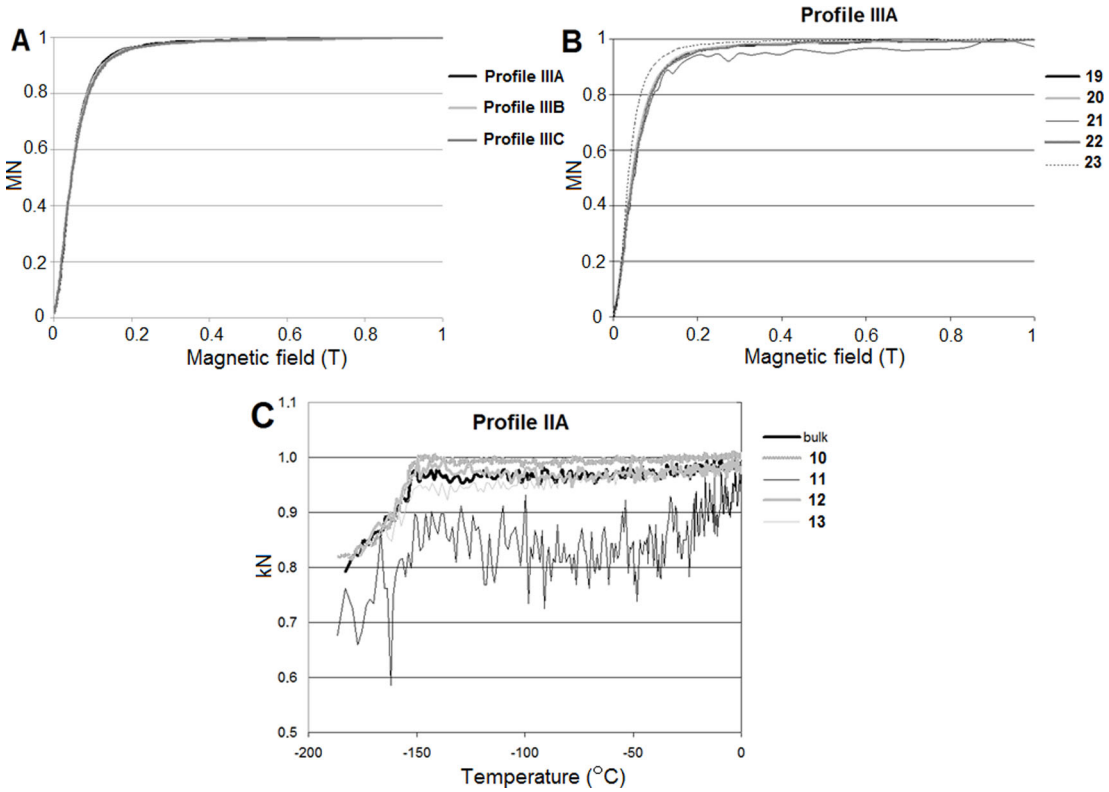

Figure 8. IRM acquisition curves (A, B) and low-temperature behaviour of magnetic susceptibility (C) of road dust obtained from selected bulk samples and snow layers (M_N, magnetization normalized by max. value; κ_N, magnetic susceptibility normalized by max. value).

the assumption that the main ferromagnetic phase is magnetite and its magnetic moment is 90–93 $Am^2\ kg^{-1}$. The saturation magnetization of magnetite was determined from the magnetic isotherms after subtraction of the paramagnetic component taken from higher magnetic fields ($H > 2T$). Fig. 11(D) depicts such an analysis for the bulk snow sample of profile IIIA.

Fig. 11 shows the magnetic susceptibility (χ) versus magnetite content (wt%) in the road dust extracted from selected snow layers of profiles IIIA and B (Figs 11A and B) and bulk snow samples obtained during third sampling campaign (profiles IIIA–C, Fig. 11C). The vertical distribution of χ and of the estimated magnetite content in profiles IIIA and B are similar, however there are marked differences for the bulk snow samples. The magnetic susceptibility of the road dust from bulk snow samples collected at 5 m distance from the road edge is higher than in the sample obtained at 15 m distance, while the estimated magnetite content is lower at 5 m than at 15 m.

3.5 Electron microscope analyses

SEM images and EDS spectra of the road dust obtained from selected bulk samples were performed to identify particles of anthropogenic and natural origin. Additionally, a feature analysis was carried out for selected road dust samples (Table 1). Three major types of anthropogenic particles were found, based on their size, shape and elemental composition: angular-shaped magnetic particles (Figs 12B–F and L), fine-grained tungsten-rich particles (Fig. 12K) and spherules (Figs 12G–I). The first and most complex group is represented by magnetite particles (Figs 12B and C), nickel-rich particles (Fig. 12D), steel (Fig. 12E) and metallic iron (Fig. 12F). The diameter of these particles ranged from 1 to 50 μm. A similar grain size has been reported by other works (Lu *et al.* 2008; Sagnotti *et al.* 2009). The fine-grained (<2 μm) particles containing tungsten were found in the form of clusters (Fig. 12K). Two types of spherules were identified in the studied samples: large silicate spherules (Figs 12G and H) with a diameter of ∼100 μm and magnetite spherules (Fig. 12I) with sizes between 10 and 50 μm. Moreover, SEM and EDS analyses also revealed the presence of sodium chloride (Fig. 12A), barium sulphate (Fig. 12L) and particles containing high amount of zinc (Fig. 12J).

Non-magnetic and magnetic minerals of natural origin (occurring in the local bedrock) such as bastnaesite (Fig. 12M), uraninite (Fig. 12N), monazite (Fig. 12O, Table 1), zircon, titanomagnetite, ilmenite, pyrite and pyrrhotite (Table 1) were found in the powders from bulk snow samples.

The highest occurrence of magnetite and other iron-rich minerals was noted in the road dust obtained from profile IC located 15 m from the road edge, while the lowest from profiles IA and IB situated 5 m and 10 m from the road edge, respectively. Furthermore, more particles of natural origin are observed in the powders from profile IA with respect to IC.

3.6 XRD, fluorescence spectrometry (WD-XRF) and Mössbauer spectroscopy

The XRD pattern and bulk chemical composition of selected road dust samples are shown in Fig. 13 and Table 2, respectively. Main crystalline phases identified in road dust obtained from bulk snow samples are: quartz (SiO_2), halite (NaCl), albite ($NaAlSi_3O_8$), biotite ($K(Mg,Fe)_3AlSi_3O_{10}(OH,F)_2$), dolomite ($CaMg(CO_3)_2$) and minor phases like phosphates ($(Fe^{3+},Al)PO_4 \bullet 3H_2O$). Moreover, the road dust is enriched in elements such as Ba, Cr, Zr, Zn, V, Sr and

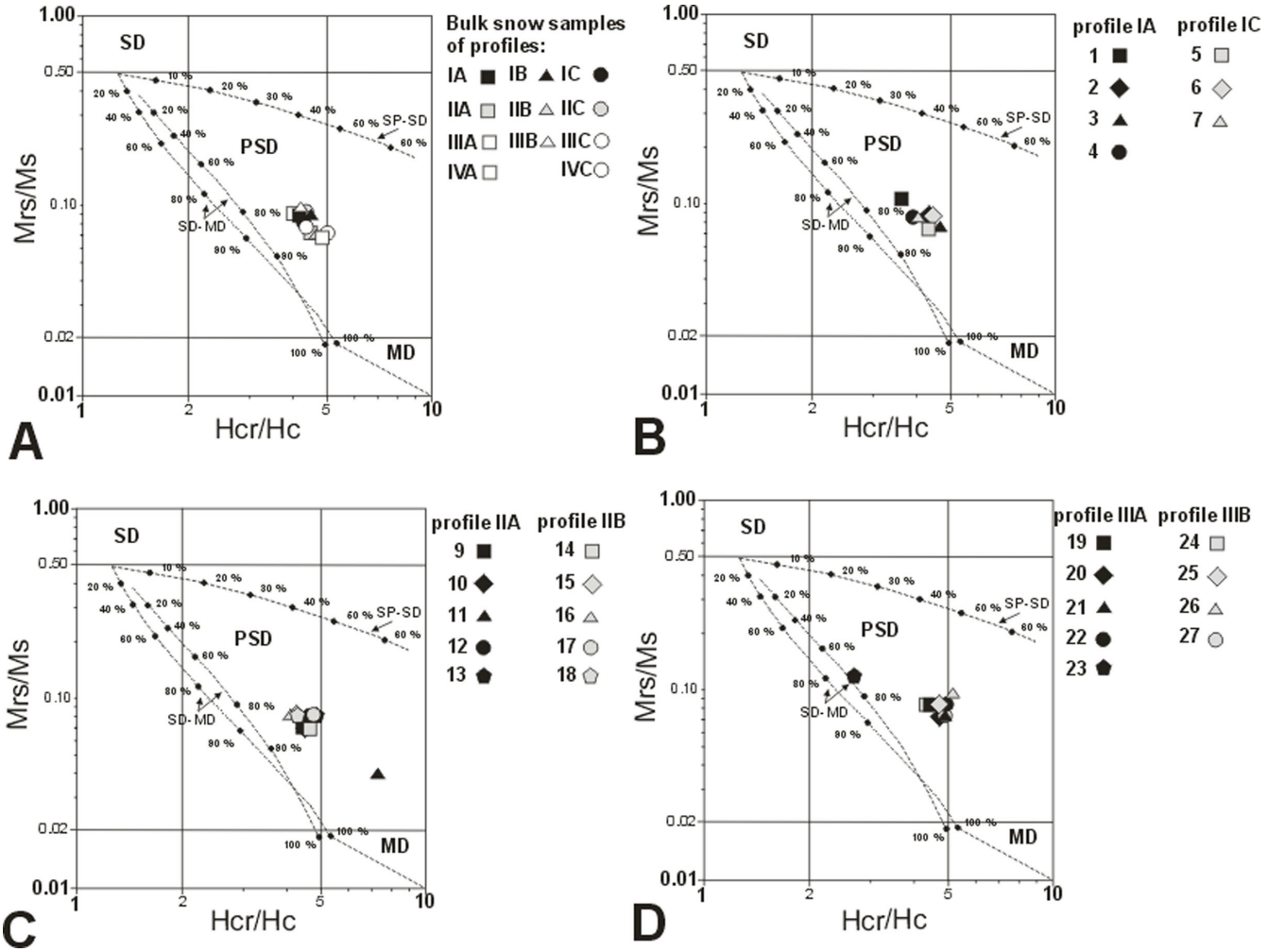

Figure 9. Day plots (Day *et al.* 1977) for road dust extracted from bulk snow samples (A) and snow layers of profiles performed during first (B), second (C) and third (D) sampling campaign. Boundaries for single-domain (SD), pseudo-single-domain (PSD) and multidomain (MD) grains and mixing lines, indicated by broken line SD/MD and SD/superparamagnetic (SP) grains are shown after Dunlop (2002).

Ce (Table 2). On the basis of WD-XRF and XRD measurements it can be concluded that the content of magnetite in the extracted road dust is far below 1 wt%, similar to what is suggested by magnetic measurements (Fig. 11).

Mössbauer spectrum at room temperature as well as at 14 K was fitted by means of three subspectra (Fig. 14) and the derived hyperfine parameters are listed in Table 3. The measured spectra include two dominant doublets that can be ascribed to biotite, in accordance with XRD, a mineral having Fe^{2+} and Fe^{3+} ions in an octahedral coordination (Table 3). There is another subspectrum showing a sign of hyperfine splitting that indicates the presence of a magnetically ordered phase. According to the values of the hyperfine parameters (Table 3), taking into account minor contribution to the overall spectra profile, the magnetically ordered phase can be ascribed to both magnetite and maghemite. Since the rock magnetic analyses indicate stoichiometric magnetite (Fig. 8C) as the dominant magnetic phase in the studied samples, the sextet component observed in Fig. 14 may be attributed to magnetite particles. Magnetite can be present as isolated particles and/or it can exist in the form of inclusions in biotite mineral (Rancourt *et al.* 2001). The ultrafine/fine (<100 nm) and coarser iron oxides can produce a similar sextet component at room temperature (Fig. 14), thus it is difficult to assess the grain size of the identified magnetite based on Mössbauer spectroscopy. The Mössbauer effect of powders from the bulk snow sample of profile IIA was lower than the road dust of profile IIIA. This reflects the fact that Mössbauer active Fe ions (i.e. magnetite and biotite) are present in lower concentration in the road dust of profile IIA.

4 DISCUSSION

Roadside snowpack accumulates traffic-related magnetic particles and their concentration increases with time during the winter season. This is expressed by the magnetic susceptibility of the entire snowpack, which increases until the late stages of melting period (Fig. 3). Higher values of magnetic susceptibility may be associated with a higher concentration of magnetic minerals (Maher 1986; Thompson & Oldfield 1986). The temporal relationship between the concentration of the magnetic particles and the snowpack thickness shows that snow is an efficient collector of magnetic particles and it can accumulate and preserve the pollutants for several months, depending on the meteorological conditions. The higher thickness of the snowpack at 5 m distance might be related to atmospheric surface layer turbulence, generated by passing vehicles and surface

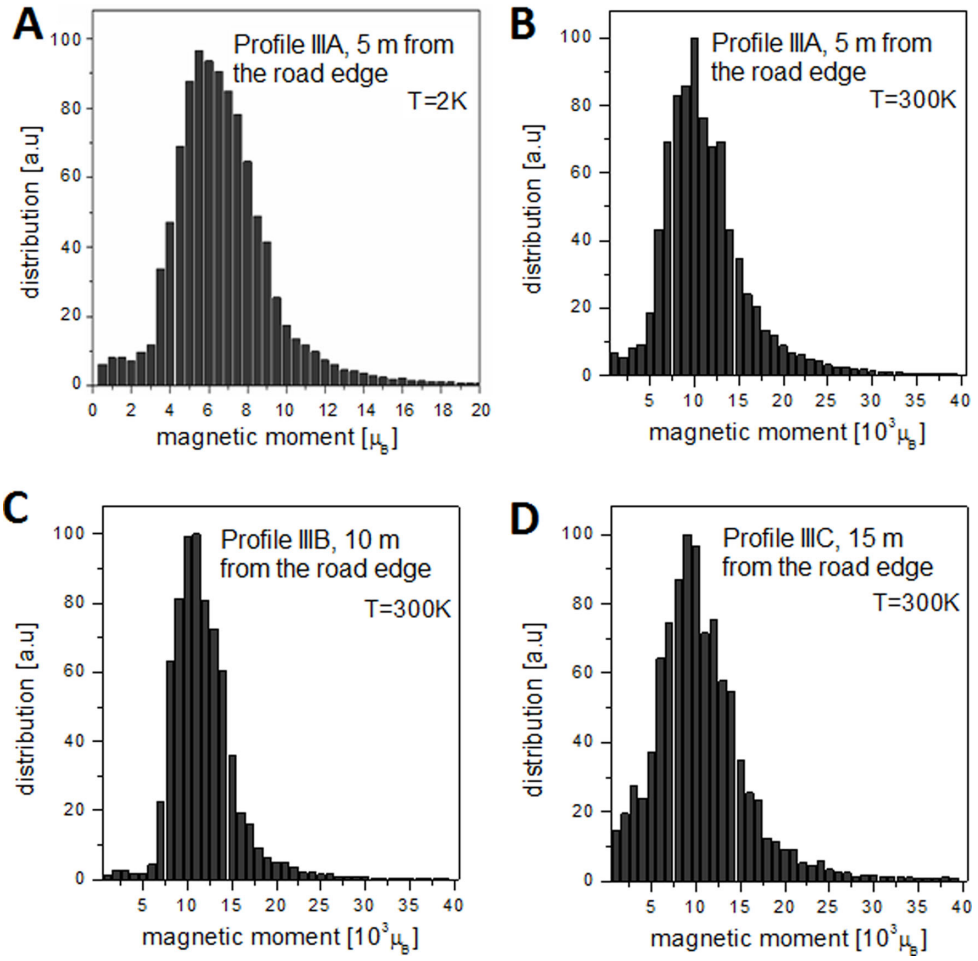

Figure 10. Distribution of magnetic moments for selected road dust samples obtained from bulk snow samples, determined from magnetic isotherms measured at $T = 2$ K (A) and $T = 300$ K (B, C, D).

microtopography at the road edge, which causes stronger accumulation of snow. Moreover, winter road maintenance (snow ploughing) may influence the snow thickness at 5 m distance.

The magnetic methods revealed that stoichiometric magnetite is the dominant ferrimagnetic mineral in all studied road dust samples (Figs 7 and 8). The saturation of IRM at about 0.2 T excludes the contribution of high-coercivity minerals, such as haematite and goethite. The dominance of magnetite in the studied road dust samples is also confirmed by the feature analysis (Table 1). Moreover, other magnetic minerals such as ilmenite, titanomagnetite and pyrrhotite have been identified in the studied road dust samples.

The decreasing trend of χ with increasing distance from the road edge was not generally observed in this data set. The highest values of χ for the studied powders were observed at the closest distance to the road edge, but at 10 m χ reached lower values than at 15 m (Figs 3 and 11C). A similar pattern was shown in one of the profiles described by Bućko *et al.* (2011); however, in this study only the top 7 cm of snow was examined. The deposition of magnetic particles on snow may be controlled by several factors, including meteorological conditions (e.g. precipitation, temperature, wind direction and speed), local topography and air turbulences generated by passing vehicles. Moreover, the deviation from the decreasing trend of χ with the increasing distance from the road may also be attributed to an increased contribution of ultrafine SP particles, which are known to have exceptionally high susceptibility (Urbat *et al.* 2004). Ultrafine magnetic particles (about 10 nm) were identified by means of the Langevin method in the road dust obtained from all bulk snow samples collected during the third sampling campaign (Fig. 10). The enhanced χ at 15 m distance could also be the result of an additional pollution source, for example, heating systems of nearby households. The distribution of the SIRM/χ ratio (Fig. 4) reaches the highest values in the road dust collected farthest from the road (15 m), suggesting the diminishing grain size of magnetic particles with increasing distance from the road. However, this pattern is not observed in the Day plots (Fig. 9A). The SIRM/χ ratio depends on the grain size and on the composition of the magnetic particles (Moreno *et al.* 2003, for analyses on magnetic powders from leaves). When the magnetic mineralogy is homogeneous, the SIRM/χ ratio shows changes in the grain size of the magnetic minerals or in the contribution from the paramagnetic minerals. Since the studied road dust is a mixture of various minerals and anthropogenic particles, it is difficult to assess the magnetic grain size distribution only through the SIRM/χ ratio. The χ and the wt% of magnetite in the road dust obtained from bulk snow samples collected at different distances from the road (Fig. 11) do not correlate. This may be associated with the presence of other iron-rich minerals (Table 1) and metals (ferromagnetic iron and nickel, Figs 12D and F, Table 1) within the studied samples, which may have a significant effect on the magnetic susceptibility.

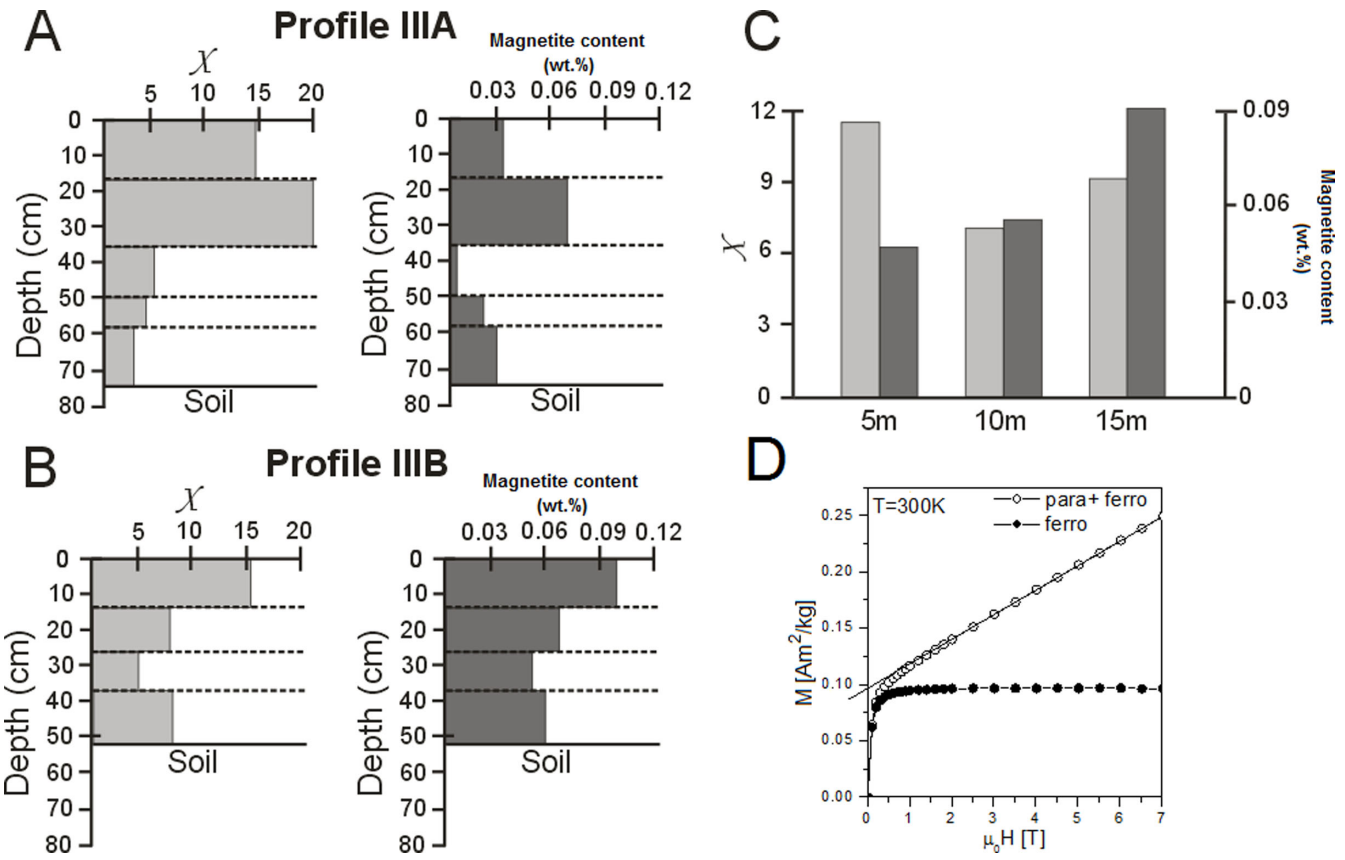

Figure 11. Mass magnetic susceptibility (χ, expressed in 10^{-8} m^3 kg^{-1}) versus magnetite content (wt%) in road dust extracted from snow layers of profiles IIIA and IIIB (A, B) and bulk samples obtained during the third sampling campaign (C). Magnetic isotherms $M(H)$ measured at $T = 300$ K for the bulk snow sample of profile IIIA (open circles) and after subtraction of paramagnetic component (closed circles) (D).

Table 1. Feature analysis of the road dust extracted from bulk snow samples collected within 5 m, 10 m and 15 m from the road edge.

Class	Profile IA		Profile IB		Profile IC	
	5 m distance from the road edge		10 m distance from the road edge		15 m distance from the road edge	
	Features					
	No.	% of total no.	No.	% of total no.	No.	% of total no.
Magnetite (Fe_3O_4)	13	24.1	9	25.7	62	50.8
Metallic iron (Fe)	3	5.6	12	34.3	4	3.3
Nickel-rich phase (+Ni)	—	—	—	—	1	0.8
Titanomagnetite (Fe_2TiO_4-Fe_3O_4)	—	—	—	—	4	3.3
Ilmenite ($FeTiO_3$)	—	—	—	—	12	9.8
Pyrrhotite (Fe_7S_8)	1	1.9	—	—	—	—
Pyrite (FeS_2)	—	—	—	—	1	0.8
Other phases containing iron (+Fe)	9	16.7	5	14.3	25	20.5
Zircon ($ZrSiO_4$)	19	35.2	8	22.9	7	5.7
Monazite ($Ce,LaPO_4$)	8	14.8	1	2.9	2	1.6
Tungsten-rich phase (+W)	1	1.9	—	—	4	3.3
Total	54	100	35	100	122	100

+, major element identified in the particle.

The vertical distribution of χ has a similar pattern to the vertical distribution of the wt% estimated for magnetite (Fig. 11), and thus this parameter in combination with detailed meteorological data (Fig. 2) can be used to distinguish and display particular accumulation periods of magnetic particles during winter as described in Section 3.1. The meteorological data show that the conditions were favourable for snow to melt on several occasions during the observation period and were likely to cause migration of particles down in the snowpack, possibly inducing the variations between χ and SIRM/χ trends (Figs 3 and 4). The SIRM/χ ratio decreases with increasing magnetic grain size for magnetite grains of sizes larger than 1 μm (Peters & Dekkers 2003). If only particles below 5 μm migrate down in the snowpack during melting conditions (Conway *et al.* 1996), then the enhanced values of SIRM/χ ratio could indicate the higher contribution of particles with a diameter between 1 and 5 μm. In the Day plot (Fig. 9), all the data (both

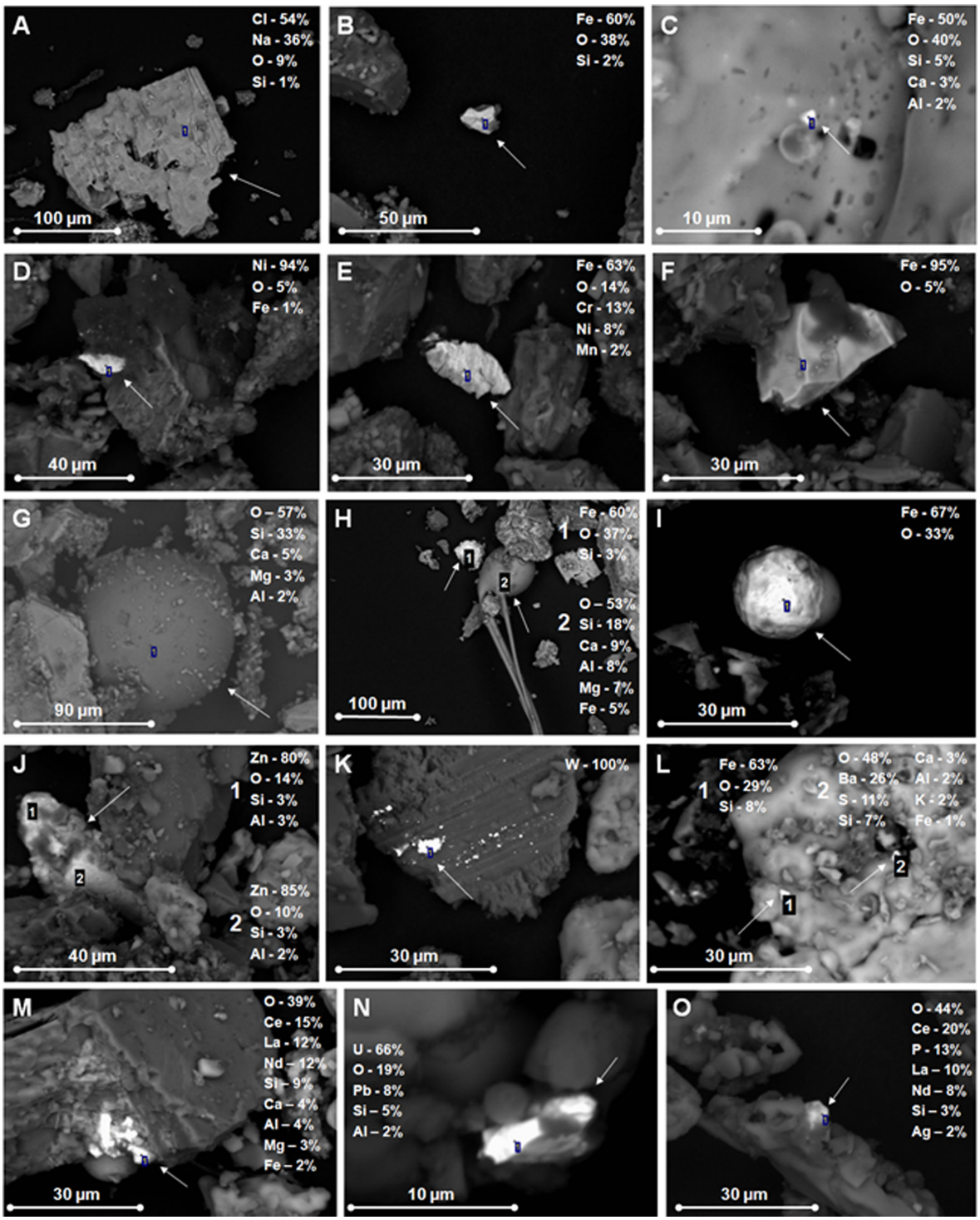

Figure 12. SEM images and chemical composition (based on EDS spectra) of selected road dust samples obtained from bulk snow samples collected at 5 m and 15 m distance from the road edge.

from the layers and from bulk samples) are very well clustered and indicate a broad mixture of SD to MD grains, the latter probably being the predominant magnetic fraction (Fig. 9). There is no apparent relationship between the distribution of SIRM/χ ratio and data points plotted on Day plot for both, powders from bulk samples and snow layers except one sample. The road dust extracted from layer 23 (profile IIIA) exhibits high values of SIRM/χ ratio and in the Day plot it is shifted towards the SD region indicating higher contribution of finer magnetic grains. The studied powders contain ultrafine magnetic particles (about 10 nm) as shown by the Langevin method (Fig. 10). Coarser magnetic grains remain in the snowpack even during melting conditions as supported by the distribution of χ with respect to the four sampling campaigns (Fig. 3). The magnetic fraction accumulated in layers 10 (profile IIA) and 15

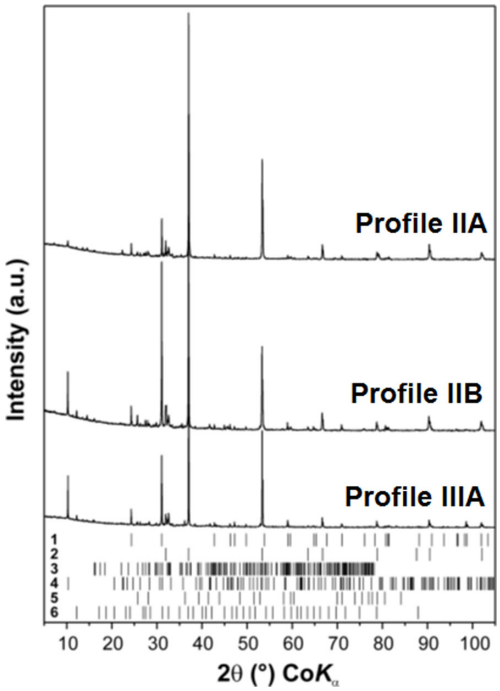

Figure 13. XRD patterns of three representative road dust samples obtained from bulk snow samples: 1, quartz (SiO_2); 2, halite (NaCl); 3, albite ($NaAlSi_3O_8$); 4, biotite ($K(Mg,Fe)_3AlSi_3O_{10}(OH,F)_2$); 5, dolomite ($CaMg(CO_3)_2$); 6, $(Fe^{3+},Al)PO_4 \cdot 3H_2O$.

(profile IIB) remains in the snow possibly till the end of the winter period and this is expressed by the distribution of χ with respect to layer 20 (profile IIIA) and 25 (profile IIIB). However, the χ values of road dust from the snow layers of the third sampling campaign are higher with respect to those from the second sampling campaign suggesting the migration of magnetic particles from the upper snow layers. The migration of the finer magnetic particles down in the snowpack is supported by the relatively higher values of SIRM/χ ratio observed in the bottom snow layer in profile IIIA.

The migration of the accumulated contaminants in the snowpack depends on its type and on several factors including thermodynamic processes (e.g. melting, freezing). Water-soluble organic substances are released early during melting since a large fraction is transported from the snow grain surfaces by early meltwater. Organic contaminants adsorbed into the particle surface tend to be released towards the end of a melt period (Meyer *et al.* 2009). Melt–freeze cycles trigger particle coagulation and snow densification, thus particle-associated chemicals are efficiently retained within the snowpack until the end of melting. Westerlund *et al.* (2011) revealed that low percentages (below 10 %) of TSS (total suspended solids) and heavy metal (Cu, Zn, Pb) loads contained in snow are transported with snowmelt, while the rest remain *in situ* with the particulate residue.

Since snowpack preserves magnetic and non-magnetic particles until the late stages of the melting period this could be considered as one of the main factors responsible for the resuspension phenomenon observed in Nordic countries. During springtime, when most of the snow and ice have melted and the surface becomes dry, the released particles are easily resuspended into the atmospheric surface layer by turbulence generated by circulating vehicles. This causes increased concentrations of urban particulate matter ($PM_{2.5}$, PM_{10}) in the air.

Table 2. Chemical composition of road dust extracted from bulk snow sample of profile IIIA. Data in Table 2 do not represent any minerals, but just chemical elements represented by their respective oxides.

Formula	Concentration (wt%)	Stat. error (%)	LLD (ppm)
SiO_2	22.57	0.24	497.1
Na_2O	21.71	0.18	317.4
Cl	12.12	0.19	247.7
Al_2O_3	5.276	0.51	263.3
CaO	1.43	0.61	54
MgO	1.08	0.63	168.9
K_2O	0.993	0.74	63.7
Fe_2O_3	0.8029	0.35	25.5
SO_3[a]	0.483	0.91	40.9
TiO_2	0.141	1.90	51.7
P_2O_5	0.0238	4.98	54.1
MnO	0.0124	5.31	27.8
CuO	0.0057	5.76	16.1
ZnO	0.0057	5.07	14.7
ZrO_2	0.0038	4.50	13.3
SrO	0.0031	5.42	10
Loss on ignition (LOI)	30		
Sum	97.2		
	(ppm)	(%)	(ppm)
Sc	4	43.00	1.6
V	14	4.57	1.7
Cr	17	8.34	3.7
Ni	5	17.30	0.8
Cu	5	4.12	1
Zn	12	2.38	0.7
Ga	1	10.50	0.2
As	2		1
Rb	5	2.48	0.3
Sr	12	1.47	0.3
Y	3	4.39	0.4
Zr	17	1.36	0.3
Nb	3	3.31	0.3
Cs	1		4.4
Ba	118	1.89	6.3
La	5		5
Ce	13	11.40	6.7
Pb	5	1.06	0.5
Th	5	7.61	0.4
U	2		0.4

[a]Included in LOI.
LLD, lower limit of detection.

SEM analyses indicate that this road dust is a mixture of natural and anthropogenic minerals. Resuspended soil and dust produced during weathering of bedrock are sources of natural non-magnetic (e.g. bastnaesite, uraninite, monazite and zircon) and magnetic (titanomagnetite, ilmenite, pyrite and pyrrhotite) minerals in the studied road dust samples (Fig. 12, Table 1). It is possible to discriminate the sources of particular anthropogenic particles on the basis of their morphological and mineralogical characteristics (Magiera *et al.* 2011). Particles containing NaCl and KCl (Figs 12A and 13) are the result of winter maintenance activities (application of de-icing substances on the roads). Angular iron-rich particles (e.g. magnetite, steel and metallic iron) are possibly generated by the abrasion of vehicle suspension components and braking system (brake linings, brake discs; Thorpe & Harrison 2008, Sagnotti *et al.* 2009). The tungsten-rich particles (Fig. 12K) identified in the roadside snow originate from the abrasion of tyre studs, which are used in

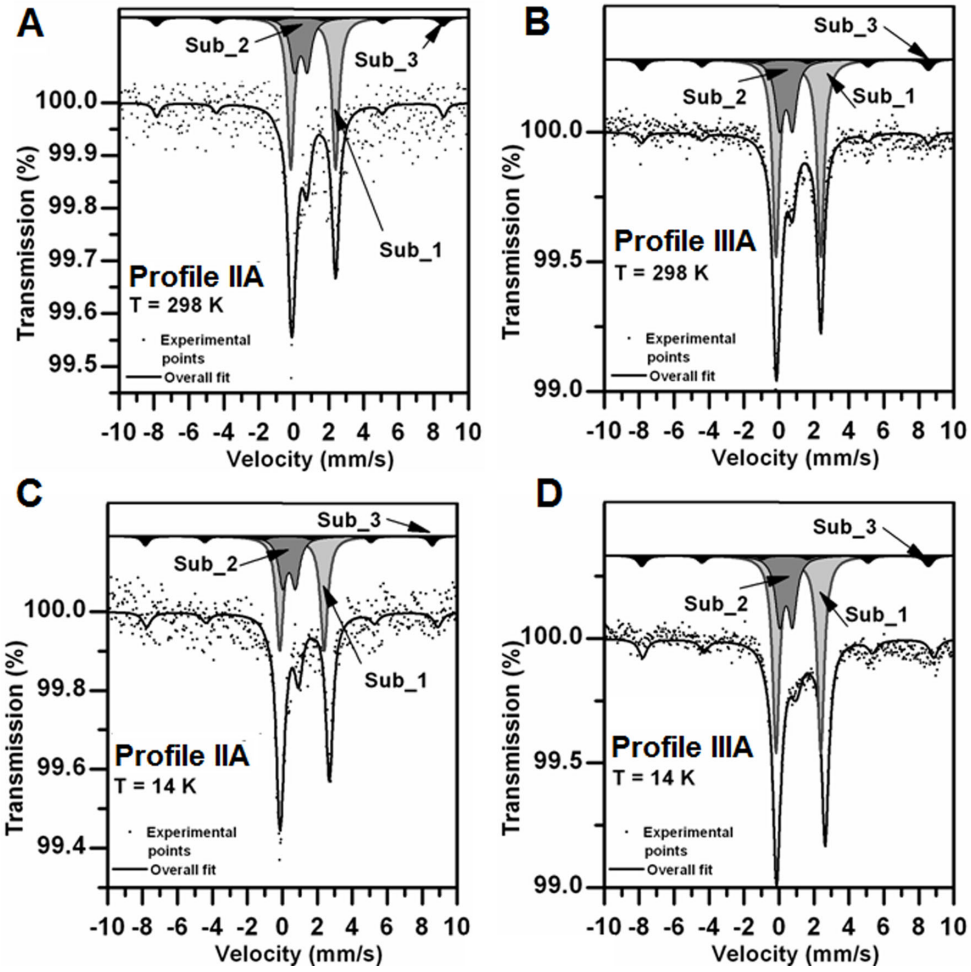

Figure 14. Zero-field Mössbauer spectra: (A, B) at room temperature and (C, D) at 14 K of road dust extracted from bulk snow samples collected from profiles IIA and IIIA.

Table 3. Hyperfine parameters of zero-field Mössbauer spectra of selected road dust samples obtained from bulk snow samples of profiles IIA and IIIA at room temperature and 14 K. T is the temperature of the measurement, δ is the isomer shift, ΔE_Q is the quadrupole splitting, B_{hf} is the magnetic hyperfine field and Γ is the linewidth.

Sample	T (K)		$\delta \pm 0.02$ (mm s^{-1})	$\Delta E_Q \pm 0.02$ (mm s^{-1})	$B_{hf} \pm 0.3$ (T)	$\Gamma \pm 0.02$ (mm s^{-1})
	298	sub_1	1.12	2.53	—	0.51
		sub_2	0.38	0.73	—	0.58
Profile IIA		sub_3	0.34	0.05	51.00	0.58
	14	sub_1	1.26	2.85	—	0.51
		sub_2	0.46	0.93	—	0.58
		sub_3	0.51	0.11	51.8	0.58
	298	sub_1	1.11	2.56	—	0.48
		sub_2	0.39	0.73	—	0.58
Profile IIIA		sub_3	0.34	0.01	51.0	0.58
	14	sub_1	1.25	2.78	—	0.50
		sub_2	0.48	0.94	—	0.61
		sub_3	0.51	0.00	51.7	0.58

most of the winter tyres sold in Finland (Peltola & Wikström 2006). Since through feature analysis (Table 1) it is possible to detect only particles whose diameter is larger than 2 μm, it was not possible to identify the tungsten-rich particles with a diameter below 1 μm, mostly observed in SEM images (Fig. 12K). The magnetic spherules (Figs 12H and I) are the products of burning processes, which are mostly related with industry, power plants and car circulation. As suggested by Magiera *et al.* (2011) the magnetic particles from coal burning usually occur in spherical forms of magnetite, maghemite or magnesioferrite. Furthermore, the spherical iron-oxides may be coated with a thin silicate or aluminosilicate layer (Fig. 12G). A coal-fired power plant is located ∼7 km south from the study site.

The road dust accumulated in a roadside snowpack contains ferrimagnetic (e.g. magnetite below 1 wt%, Fig. 11) as well as dia/paramagnetic minerals (e.g. quartz, albite, halite, biotite, Fig. 13, Table 2). The content of each group of minerals (dia/para/ferromagnetic *sl*) in certain snow layers could change due to migration process ongoing during melting. This may explain the variations of magnetic parameters of road dust samples extracted from the same snow layer collected during two different consecutive sampling campaigns (e.g. layers 10, 20 and 15, 25, Fig. 3).

The identified anthropogenic particles have a grain size ranging from 10 nm up to ∼300 μm (Figs 10, 12 and 14). The grain size of these particles determines in which parts of the respiratory system the particles are deposited. Particles below 1 μm are inhaled deeper in the respiratory system, thus having an adverse effect on health. Moreover, they may trigger health consequences other than respiratory health effects, since they can accumulate heavy metals due to their large active surface. The exposure to traffic-generated particulate matter including iron-oxides may be related with the

development and progression of atherosclerosis (e.g. Hoffmann *et al.* 2007; Zhu *et al.* 2011).

5 CONCLUSIONS

This study displays the spatio-temporal variations of the magnetic parameters (χ, SIRM/χ) of dust accumulated in a roadside snowpack. χ reaches the highest values in the samples collected closest to the road (5 m). However, χ decreases at 10 m and slightly increases at farthest distance from the road (15 m). The horizontal distribution of SIRM/χ ratio suggests the diminishing grain size of magnetic particles with increasing distance from the road. The concentration of the magnetic particles increases in a snowpack during winter as expressed by the distribution of the mass magnetic susceptibility. The snowpack preserves the magnetic and non-magnetic particles until the beginning of strong melting, and this aspect can trigger the resuspension phenomenon characteristic to Nordic countries during springtime. The distribution of χ and SIRM/χ ratio may indicate the migration of magnetic particles down in the snowpack during melting conditions. However, due to heterogeneous mineralogical composition of the studied powders neither parameter can be used to clearly explain this phenomenon. A mixture of fine-grained to coarse-grained magnetite was identified as the primary magnetic mineral in all the studied road dust samples. Furthermore, the contribution of ultrafine iron-oxides (about 10 nm) was confirmed by the application of the Langevin method. The content of magnetite has been estimated below 1 wt%. The XRD and WD-XRF analyses revealed high content of dia/paramagnetic natural (e.g. quartz, albite, biotite) and anthropogenic (sodium chloride) particles. As indicated by SEM measurements, the roadside snowpack is enriched in anthropogenic particles such as angular and spherical iron-oxides, tungsten-rich particles and sodium chloride. Since some of these particles are less than 1 μm in diameter they may pose serious threats to human health.

This research shows that road traffic is a significant source of particulate matter of specific magnetic, morphological and mineralogical properties, mostly due to non-exhaust emissions such as the abrasion of road surface, vehicle components and tyre studs often used in northern Europe. Since the effects of tungsten-rich particles in air, surface and ground water quality are relatively poorly known this leads to an open question whether the quality of the environment could be improved by restricting the use of studs in winter tyres.

This work encourages further investigation of the applied methodology for quantifying the traffic-related particles. Future improvements can be applied to the sampling methodology, especially during rapid melting period, when the re-distribution of the particles is most intensive. Simultaneously with the sampling of the snow, the topsoil can be analysed to monitor the migration of particles and to verify if frozen ground would stop the migration. The modeling of snow infiltration processes would also greatly benefit the described methodology in understanding the possible losses of the material during melting events. To better understand the phenomena of magnetic particle migration in the snowpack other relevant magnetic parameters should be applied in future studies.

ACKNOWLEDGEMENTS

This research was financially supported by Vilho, Yrjö and Kalle Väisälä Foundation (Finnish Academy of Science and Letters) and Academy of Finland, project 140939 ‘Impacts of climate change on snow properties and snow cover’. The authors gratefully acknowledge the support by the Czech Science Foundation (GACR P108-11-1350), the internal grant of Palacky University in Olomouc, Czech Republic (PrF_2013_014), and the Operational Program Research and Development for Innovations-European Regional Development Fund (project CZ.1.05/2.1.00/03.0058) and Operational Program Education for Competitiveness–European Social Fund (project CZ.1.07/2.3.00/20.0017) of the Ministry of Education, Youth and Sports of the Czech Republic. We also thank Jiři Tuček for assistance in preparation of this manuscript and Robert Klein for correcting the English text. Comments and suggestions made by the two reviewers (Aldo Winkler and Marcos A. E. Chaparro) are highly appreciated.

REFERENCES

Bućko, M.S., Magiera, T., Pesonen, L.J. & Janus, B., 2010. Magnetic, geochemical, and microstructural characteristics of road dust on roadsides with different traffic volumes: case study from Finland, *Water, Air, Soil Pollut.,* **209**(1–4), 295–306.

Bućko, M.S., Magiera, T., Johanson, B., Petrovský, E. & Pesonen, L.J., 2011. Identification of magnetic particulates in road dust accumulated on roadside snow using magnetic, geochemical and micro-morphological analyses, *Environ. Pollut.,* **159**(5), 1266–1276.

Chaparro, M.A.E., Marié, D.C., Gogorza, C.S.G., Navas, A.M. & Sinito, A.M., 2010. Magnetic studies and scanning electron microscopy: x-ray energy dispersive spectroscopy analyses of road sediments, soils, and vehicle derived emissions, *Stud. Geophys. Geod.,* **54,** 633–650.

Chrobak, A., Haneczok, G., Chełkowska, G., Kassiba, A. & Ziółkowski, G., 2011. Numerical analysis of superparamagnetic clusters, *Phys. Status Solidi A.,* **208**(11), 2692–2698.

Conway, H., Gades, A. & Raymond, C.F., 1996. Albedo of dirty snow during conditions of melt, *Water Resour. Res.,* **32**(6), 1713–1718.

Day, R., Fuller, M. & Schmidt, V.A., 1977. Hysteresis properties of titanomagnetites: grain size and compositional dependence, *Phys. Earth planet. Inter.,* **13**(4), 260–267.

Dunlop, D.J., 2002. Theory and application of the day plot (Mrs/Ms versus Hcr/Hc) 1. Theoretical curves and tests using titanomagnetite data, *J. geophys. Res.,* **107**(B3), 1–22.

Fabian, K., Reimann, C., McEnroe, S.A. & Willemoes-Wissing, B., 2011. Magnetic properties of terrestrial moss (Hylocomium splendens) along a north–south profile crossing the city of Oslo, Norway, *Sci. Total Environ.,* **409,** 2252–2260.

Fierz, C. *et al.*, 2009. The international classification for seasonal snow on the ground. IHP-VII Technical Documents in Hydrology N°83, IACS Contribution N°1. UNESCO-IHP, Paris.

Hautala, E.L., Rekilä, R., Tarhanen, J. & Ruuskanen, J., 1995. Deposition of motor vehicle emissions and winter maintenance along roadside assessed by snow analyses, *Environ. Pollut.,* **87**(1), 45–49.

Hoffmann, B. *et al.*, 2007. Residential exposure to traffic is associated with coronary atherosclerosis, *Circulation,* **116**(5), 489–496.

Kakay, A., Gutowski, M.W., Takacs, L., Franco, V. & Varga, L.K., 2004. Langevin granulometry of the particle size distribution, *J. Phys. Math. Gen.,* **37**(23), 6027–6042.

Katsushima, T., Kumakura, T. & Takeuchi, Y., 2009. A multiple snow layer model including a parameterization of vertical water channel process in snowpack, *Cold Regions Sci. Tech.,* **59**(2–3), 143–151.

Lu, S.G., Zheng, Y.W. & Bai, S.Q., 2008. A HRTEM/EDX approach to identification of the source of dust particles on urban tree leaves, *Atmos. Environ.,* **42,** 6431–6441.

Magiera, T., Jabłońska, M., Strzyszcz, Z. & Rachwał, M., 2011. Morphological and mineralogical forms of technogenic magnetic particles in industrial dusts, *Atmos. Environ.,* **45**(25), 4281–4290.

Maher, B., 1986. Characterization of soils by mineral magnetic measurements, *Phys Earth planet. Inter.,* **42**(1–2), 76–92.

Meyer, T., Lei, Y.D., Muradi, I. & Wania, F., 2009. Organic contaminant release from melting snow. 1. Influence of chemical partitioning, *Environ. Sci. Tech.,* **43**(3), 657–662.

Moreno, E., Sagnotti, L., Dinares-Turell, J.D., Winkler, A. & Cascella, A., 2003. Biomonitoring of traffic air pollution in Rome using magnetic properties of tree leaves, *Atmos. Environ.,* **37**(21), 2967–2977.

Parks, G.A. & Akhtar, S., 1968. Magnetic moment of Fe^{2+} in paramagnetic minerals, *Am. Mineral.,* **53,** 406–415.

Peltola, P. & Wikström, E., 2006. Tyre stud derived tungsten carbide particles in urban street dust, *Boreal Environ. Res.,* **11**(3), 161–168.

Peters, C. & Dekkers, M.J., 2003. Selected room temperature magnetic parameters as a function of mineralogy, concentration and grain size, *Phys. Chem. Earth,* **28,** 659–667.

Rancourt, D.G., Mercier, P.H.J., Cherniak, D.J., Desgreniers, S., Kodama, H., Robert, J.L. & Murad, E., 2001. Mechanisms and crystal chemistry of oxidation in annite: resolving the hydrogen-loss and vacancy reactions, *Clays Clay Miner.,* **49**(6), 455–491.

Sagnotti, L., Taddeucci, J., Winkler, A. & Cavallo, A., 2009. Compositional, morphological, and hysteresis characterization of magnetic airborne particulate matter in Rome, Italy, *Geochem. Geophys. Geosyst.,* **10,** Q08Z06, doi:10.1029/2009GC002563.

Salo, H., Bućko, M.S., Vaahtovuo, E., Limo, J., Makinen, J. & Pesonen, L.J., 2012. Biomonitoring of air pollution in SW Finland by magnetic and chemical measurements of moss bags and lichens, *J. Geochem. Explor.,* **115,** 69–81.

Sansalone, J.J. & Glenn, D.W., 2002. Accretion of pollutants in snow exposed to urban traffic and winter storm maintenance activities. I, *J. Environ. Eng.,* **128**(2), 151–166.

Thompson, R. & Oldfield, F., 1986. *Environmental Magnetism,* Allen & Unwin, London, 227 pp.

Thorpe, A. & Harrison, R.M., 2008. Sources and properties of non-exhaust particulate matter from road traffic: a review, *Sci. Total Environ.,* **400**(1–3), 270–282.

Urbat, M., Lehndorff, E. & Schwark, L., 2004. Biomonitoring of air quality in the Cologne conurbation using pine needles as a passive sampler—Part I: magnetic properties, *Atmos. Environ.,* **38**(23), 3781–3792.

Viklander, M., 1998. Snow quality in the city of Lulea, Sweden-time-variation of lead, zinc, copper and phosphorus, *Sci. Total Environ.,* **216**(1–2), 103–112.

Viklander, M., 1999. Substances in urban snow. A comparison of the contamination of snow in different parts of the city of Lulea, Sweden, *Water, Air, Soil Pollut.,* **114**(3–4), 377–394.

Viskari, E.L., Rekilä, R., Roy, S., Lehto, O., Ruuskanen, J. & Kärenlampi, L., 1997. Airborne pollutants along a roadside: assessment using snow analyses and moss bags, *Environ. Pollut.,* **97,** 153–160.

Westerlund, C., Viklander, M., Nordqvist, K., Galfi, H. & Marsalek, J., 2011. Particle pathways during urban snowmelt and mass balance of selected pollutants, in *Proceedings of 12th International Conference on Urban Drainage,* Porto Alegre/Brazil, pp. 1–7.

Zhu, M.T. *et al.*, 2011. Endothelial dysfunction and inflammation induced by iron oxide nanoparticle exposure: risk factors for early atherosclerosis, *Toxicol Lett.,* **203**(2), 162–171.